

Dark Matter Through the Neutrino Portal

Adam Falkowski, José Juknevich, and Jessie Shelton

*Department of Physics
Rutgers University
Piscataway, NJ 08854*

Abstract

We consider a model of dark matter whose most prominent signature is a monochromatic flux of TeV neutrinos from the galactic center. As an example of a general scenario, we consider a specific model where the dark matter is a fermion in the adjoint representation of a hidden $SU(N)$ gauge group that confines at GeV energies. The absence of light fermionic states in the dark sector ensures stability of dark matter on cosmological time scales. Dark matter couples to the standard model via the neutrino portal, that is, the singlet operator HL constructed from the Higgs and lepton doublets, which is the lowest dimensional fermionic singlet operator in the standard model. This coupling prompts dark matter decay where the dominant decay channel has one neutrino (and at least one dark glueball) in the final state. Other decay channels with charged standard model particles involve more particles in the final state and are therefore suppressed by phase space. In consequence, the standard indirect detection signals like gamma-ray photons, antiprotons and positrons are suppressed with respect to the neutrino signal. This coupling via the neutrino portal is most robustly constrained by Super-Kamiokande, which restricts the dark matter lifetime to be larger than 10^{25} seconds. In the near future, the scenario will be probed by the new generation of neutrino telescopes. ANTARES will be sensitive to a dark matter lifetime of order 10^{26} seconds, while IceCube/DeepCore can probe a lifetime as large as 10^{27} seconds.

1 Introduction

There is widespread hope that the next few years will see the detection of a dark matter particle. Signals of dark matter are searched for obliquely in colliders, directly in underground detectors, and indirectly in cosmic rays. Of these three methods, the last one is *a priori* the most challenging because backgrounds from astrophysical processes are difficult to estimate. Nevertheless, indirect detection is a topic of great current interest due to rapid instrumental progress and a constant flow of new and exciting data. During the past year, interest in indirect detection has been further amplified by tantalizing signals from the PAMELA [1], ATIC [2] and FERMI [3] experiments, which may or may not be hints of dark matter.

The main search channels for indirect dark matter detection are cosmic ray photons, antiprotons, positrons, and neutrinos. Certain features of neutrinos make them an especially clean detection channel. Neutrinos, like photons, have no electric charge and traverse our galaxy along straight paths. Therefore the flux of neutrinos observed at the Earth is determined in a straightforward way by the production mechanism and is free of the astrophysical uncertainties which plague the propagation of charged particles. Neutrinos have a further advantage over photons in that astrophysical neutrino backgrounds are far less severe. Detection of a large diffuse flux of astrophysical neutrinos would thus constitute a smoking gun for dark matter.

In spite of these attractive features, neutrinos are seldom singled out as a primary dark matter discovery channel. Neutrinos are weakly interacting and require large, dedicated experiments to detect. It is much easier to detect charged particles and photons. Typical models of dark matter encountered in the literature predict a cosmic neutrino flux that is smaller than or comparable to the fluxes in other observable channels. Most often, dark matter dominantly annihilates or decays into other standard model particles— W bosons, for instance, or tau leptons—which produce neutrinos when they subsequently decay. But then one would expect to first detect that dark matter signal by observing antiprotons from W decays or gamma ray photons from π^0 s in the tau lepton decay chain. Annihilation or decay to primary, hard neutrinos typically appears as only one of several possible final states. The $SU(2)$ gauge symmetry of the standard model generically implies that charged particles are produced at comparable rates, and those lead to more accessible signals. For these reasons measurement of the cosmic neutrino flux sometimes provides useful constraints on dark matter models [4, 5], or may serve to break a degeneracy among different models once a signal is detected in another channel, but is not considered the main discovery channel.

In this paper we argue that one can construct dark matter models which predict a cosmic

neutrino flux that is more prominent than the antiproton, positron and gamma ray fluxes. If such a model is realized in nature, the indirect detection signal could first show up in neutrino telescopes. The neutrino flux from the galactic center can well be larger than the atmospheric neutrino background, leading to a sharp smoking-gun signature. The current generation of neutrino telescopes (IceCube and ANTARES) or the future one (KM3NET) may become the discovery machines.

What kind of set-up is required for dark matter to produce a large neutrino flux? It is plausible that the dark matter particle is a perfect singlet under the standard model gauge interactions. If such is the case it can couple to the visible sector via gauge singlet operators which can be constructed out of standard model fields. The lowest dimensional singlet operators are the Higgs mass $|H|^2$ and the hypercharge field strength $B_{\mu\nu}$, both of mass dimension 2. Dark matter coupling through the Higgs portal or via kinetic mixing with hypercharge has been explored in numerous models. However, if the dark matter particle is a *fermion*, then the lowest dimensional standard model operator it can couple to is the dimension 5/2 operator

$$HL \equiv \epsilon_{ab} H^a L^b = H^+ e_L^- - H^{0*} \nu_L = G^+ e_L^- - \frac{1}{\sqrt{2}}(v + h + iG^0)\nu_L \quad (1)$$

where $v = 246$ GeV is the standard model Higgs vev. We refer to this operator as *the neutrino portal*.¹

Now, suppose that the fermionic dark matter particle λ is a part of a larger dark sector that is neutral under the standard model gauge group. Assume that the dark sector couples to the standard model via the neutrino portal as

$$\mathcal{L}_{int} = O_{dark}(\lambda)(LH) \quad (2)$$

where $O_{dark}(\lambda)$ is a fermionic gauge singlet operator constructed from the dark matter particle λ and other fields in the dark sector. Suppose in addition that the dark sector contains *bosonic* states that are lighter than λ . If λ is the lightest *fermionic* state in the dark sector, it is stable within the dark sector. But in the presence of the coupling Eq. (2) the dark matter particle is allowed to decay into fermionic states in the standard model. The leading dark matter decay channel is then

$$\lambda \rightarrow (\text{Dark}) + \nu \quad (3)$$

which leads to a neutrino flux as the dominant signal from dark matter decay! Moreover, if there is only one dark sector particle in the final state, the neutrino flux is monochromatic.

¹The coupling through the neutrino portal has been previously utilized in models of dark matter in a somewhat different context [6].

Of course, the coupling in Eq. (2) also predicts other, subdominant decay channels: $\lambda \rightarrow (\text{Dark}) + (h\nu, W^\pm e^\mp, Z\nu)$, which imply charged particle fluxes. But these other decays have one more particle in the final state, and are therefore suppressed by phase space. The branching ratio for these states with on-shell bosons depends on the multiplicity of dark particles in the final state and the mass of the dark matter particle, and can be made as small as 10^{-2} . Cosmic neutrinos then become the most prominent signal of dark matter decay.

We present here a simple model with a strongly coupled dark sector which explicitly realizes this idea. The model contains an $SU(N)$ dark gauge group plus a massive Majorana fermion in the adjoint representation. With this low energy spectrum the dark gauge group is asymptotically free for any N . Therefore the dark color is confined at low energies and the physical states are dark color singlets: glueballs and glueballinos (bound states of the adjoint fermion and gluons). The lightest, ground state glueballino (in the following simply called the glueballino) is our dark matter candidate. Note that the glueballino, being fermionic, cannot decay solely into glueballs, even if it is heavier. We assume that the dark confinement scale is in the (sub)-GeV ballpark which sets the mass scale for the glueballs, while the glueballino mass is set by the Majorana mass of the adjoint fermion of order 1-5 TeV. In the absence of any coupling between the dark sector and the standard model the glueballino would be perfectly stable. Decay channels open up once the adjoint fermion is coupled to the standard model via the neutrino portal, that is, via the dimension six coupling $\frac{c}{\Lambda_N^2} \text{Tr}[G_{\mu\nu} \bar{\lambda}] \sigma_{\mu\nu} (LH)$. For $\Lambda_N \sim 10^{14} - 10^{15}$ GeV and $c \sim 1/16\pi^2$ (a one-loop factor) the dark matter lifetime is much longer than the age of the universe, while at the same time the decay rate is large enough to yield observable signals. The leading decay of dark matter is the two-body decay into a dark gluon and a neutrino. This results in a flux of monochromatic neutrinos from the galactic center which can be detected in the current generation of neutrino telescopes, ANTARES and IceCube. Other indirect detection signals are suppressed, so that neutrino telescopes are singled out as the most sensitive probes of our scenario. Moreover, the cross-section of our dark matter particle on nuclei is small, giving null predictions for direct detection experiments.

The paper is organized as follows. In section 2 we introduce our example model of the dark sector and discuss the spectrum after the dark gauge group confines. In section 3 we study the thermal relic abundance, including the Sommerfeld effect and late annihilation of glueballinos. Depending on assumptions about modeling nonperturbative contributions to the annihilation cross-section, the correct relic abundance may be obtained for dark matter masses in the range 1-10 TeV provided the strong coupling scale is sufficiently small. Besides the sizable theoretical uncertainties due to modeling the strongly coupled

effects at energies below the confinement scale, the precise value of the mass is also sensitive to the number of degrees of freedom in the hidden sector – the larger the number of colors, the smaller the required dark matter mass. In section 4 we compute the decay width and the branching ratio for dark matter decays due to the coupling via the neutrino portal. We demonstrate that for the dark matter mass close to a TeV the neutrino decay channel is by far dominant, while other decay channels have branching ratios at a few percent level. For heavier dark matter, close to 5 TeV, the decay rate into charged standard model particles becomes comparable to the decay rate into neutrinos. In section 5 we make a slight detour to explain why the glueballs in the dark sector cannot be stable. We enumerate various options for their decay into the standard model final states and indicate options for model building. Glueball decays may do lead to additional indirect detection signals which however are highly model dependent. For this reason we choose to focus on the more robust signals from the glueballino decays via the neutrino portal.

In the later sections of the paper we turn to discussing observational consequences of the general scenario where structure in the dark sector enables dark matter decay to yield a monochromatic neutrino flux as its primary signal. In section 6 we determine the parameter space consistent with indirect detection experiments. The Super-Kamiokande bounds on the neutrino flux from the galactic center set a lower bound on the dark matter lifetime, or equivalently on the scale Λ_N which suppresses the coupling through the neutrino portal. That scale turns out to lie in the 10^{15} GeV ballpark—the typical scale for lepton violating interactions. We also study the current bounds from the antiproton, positron and gamma ray fluxes. We conclude that even for the maximum lifetime allowed by Super-Kamiokande the indirect bounds from other detection channels are less constraining in a large portion of parameter space. One exception are the bounds from antiprotons, which are produced in subdominant dark matter decay channels with standard model gauge and Higgs boson in the intermediate state. These bounds are comparable to those from Super-Kamiokande for dark matter masses around 1 TeV, and when the dark matter mass is close to 5 TeV (and thus the branching ratio for decays into charged particles becomes large) the antiproton flux measured by the PAMELA experiment implies a more severe constraint on the dark matter decay rate than the Super-Kamiokande bounds. However, one should note that uncertainties involved in the propagation of antiprotons in our galaxy are very large, and by changing the parameters of the propagation model one can reduce the antiproton flux by a factor of five, thus obliterating the antiproton bounds. We therefore continue to refer to the Super-Kamiokande bounds, which are comparatively free of astrophysical uncertainties. In section 7 we study the discovery prospects in ANTARES and IceCube. We compute the rate of signal events in both detectors induced by the predicted neutrino flux from the

galactic center, and compare it to the background rate from atmospheric neutrinos. We conclude that neutrino telescopes have a great potential to probe this scenario, and their sensitivity will exceed that of Super-Kamiokande by 1-2 orders of magnitude.

2 Model of Dark Sector

In this section we construct an example of a dark matter model which leads to an enhanced neutrino signal. The model falls into the *hidden valley* class [7], where the hidden sector contains fairly light states (here GeV scale) interacting very weakly with the standard model through higher dimensional operators. The hidden sector here consists of a $SU(N)$ gauge group together with a fermion in the adjoint representation, λ^a . Incidentally, this is also the field content of pure $\mathcal{N} = 1$ super-Yang-Mills theory, but we do not consider supersymmetry here: the fermion has a TeV scale mass m_λ and the interactions of the hidden sector with the standard model are not supersymmetric.

The dark gauge group is asymptotically free for any N so that the theory confines at low energies. We assume that the confinement scale is in the GeV ballpark, well below the adjoint fermion mass. The low-energy theory below a TeV contains only the dark gluons, and after confinement the low-energy degrees of freedom are stable glueballs. The spectrum of a pure Yang-Mills theory has been studied on the lattice for the case $N = 3$ [8]. These studies indicate there are 12 stable glueballs in a pure $SU(3)$ theory, labeled by their J^{PC} quantum numbers. The masses of the glueballs are set by the strong coupling scale Λ . The lightest glueball is the 0^{++} , with $m_{0^{++}} = 4.2r_0^{-1}$ where r_0^{-1} is the “force radius” related to the confinement scale Λ (defined by the running coupling in the MS-bar scheme) by $\Lambda = 0.62r_0^{-1}$ [9]. Thus, the lightest glueball mass

$$m_{0^{++}} \approx 7\Lambda \tag{4}$$

is appreciably larger than the confinement scale. The spectrum of glueball states for $N = 3$ is shown in figure 1. While lattice results for the glueball spectrum are only available for $N = 3$, the masses of glueballs do not vary appreciably with N in the large- N limit. The spectrum of the $N = 3$ theory is thus a useful benchmark for more general cases.

In addition to glueballs, the spectrum of the dark sector contains color singlet bound states of the adjoint fermion and gluons. Borrowing from supersymmetric jargon we refer to the lightest of such states as *the glueballino*. The glueballino is stable under decays within the dark sector, and is our dark matter candidate.

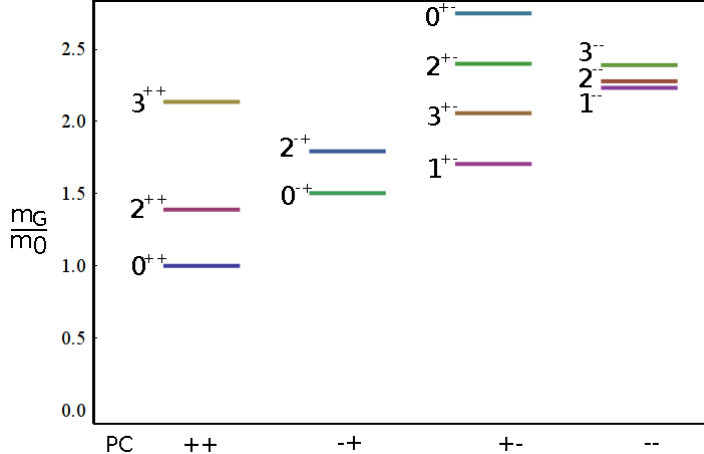


Figure 1: Glueball spectrum for pure $SU(3)$ gauge theory, after [8]. Masses are shown in units of the lightest glueball mass m_0 .

3 Relic Abundance of Dark Matter

In the early universe at $T > 1$ TeV the adjoint fermions and the dark gluons were in thermal equilibrium. We assume that at even larger temperatures the dark sector was in thermal equilibrium with the standard model, but near a TeV the two sectors are already decoupled. Below a TeV the adjoint fermions become non-relativistic and drop out of thermal equilibrium, leaving a relic abundance that is in principle determined by the fermion mass, the dark gauge coupling and the number of dark colors. The freezeout calculation of λ abundance is closely analogous to the well-studied problem of gluino dark matter [10, 11]. In the following we estimate the range of fermion masses that are compatible with the observed dark matter abundance.

We first compute the relic abundance ignoring non-perturbative effects, in which case the standard textbook procedure applies. The perturbative matrix element for the annihilation $\lambda\lambda \rightarrow gg$ can be found in [12]. At low energies the thermally averaged annihilation cross-section is given by

$$\langle\sigma_{ann}v\rangle \approx \frac{3N^2}{4(N^2 - 1)} \frac{\pi\alpha_d^2}{m_\lambda^2} \quad (5)$$

where α_d is the dark coupling at the scale m_λ , given in terms of the confinement scale and the number of dark colors by $\alpha_d = 6\pi/11N \log(m_\lambda/\Lambda)$. Integrating the Boltzmann equation relates the annihilation cross section to the relic abundance Y_∞ . The latter can be translated into the dark matter density fraction today by $\Omega_\lambda \approx Y_\infty m_\lambda s_0 / \rho_{crit}$ where $s_0 = 2889.2/\text{cm}^3$, $\rho_{crit} = 3.95 \times 10^{-47} \text{ GeV}^4$; WMAP fixes Ω_λ to be 0.23 [13]. The final result strongly depends on the number of dark colors (the number of degrees of freedom in the hidden sector). Our results are plotted in Fig. 2.

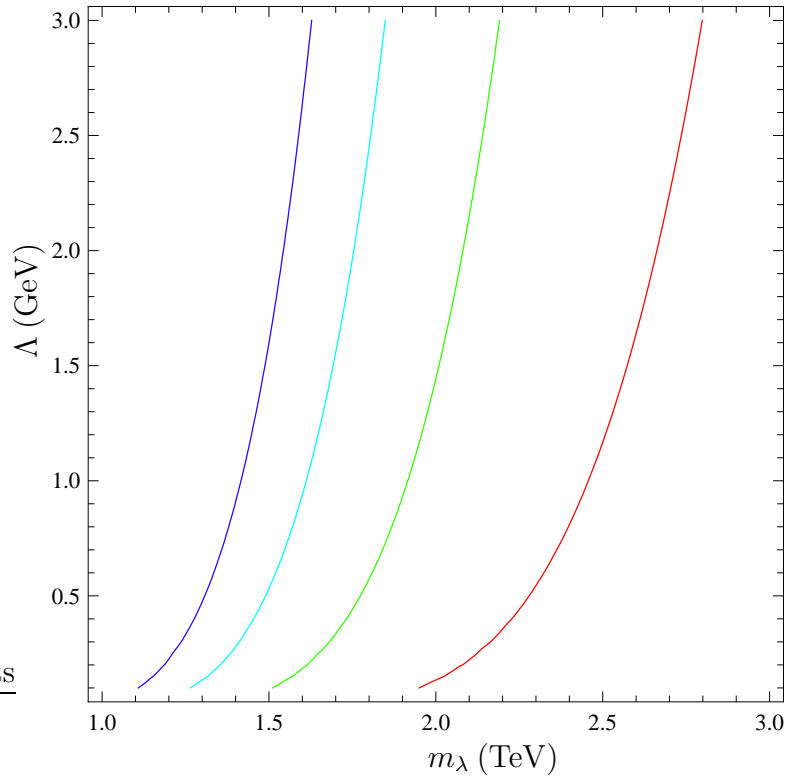


Figure 2: Contours of relic density $\Omega_\lambda = .23$ in the m_λ - Λ/m_λ plane, for $N = 3$ (red), $N = 4$ (green), $N = 5$ (cyan), $N = 6$ (blue). Using the perturbative annihilation cross-section.

Nonperturbative contributions to the annihilation cross-section are significant and introduce large uncertainties [10, 11, 14]. Below we estimate the effects of Sommerfeld enhancement and of enhanced annihilation after confinement.

The exchange of dark gluons between the nonrelativistic fermions leads to an enhanced annihilation cross section at low velocity [15]. The Coulomb interaction of two massive particles takes place on a time scale set by the energy of the scattering particles, $\tau_{\lambda\lambda} \sim (m_\lambda v^2)^{-1} \sim 1/T$. Meanwhile, the time scale for a massive particle to interact with a gluon in the thermal bath, and therefore to randomize its color, is set by its mean free path in the thermal bath. This can be estimated by $\tau_{\lambda g} = \ell = (n_g \langle \sigma_{g\lambda} v \rangle)^{-1} \sim m_\lambda^2/T^3$. Since $\tau_{\lambda\lambda} \ll \tau_{\lambda g}$, the two gluinos will remain in a state of definite total color throughout the interaction, and the sign and strength of their interaction will depend on that particular color state. We can solve the Schrödinger equation in the basis of definite total color, and derive the Sommerfeld enhancement in each color representation subspace i . Two particles of equal mass moving in a non-Abelian Coulomb potential have a scattering amplitude enhanced from the plane wave result by the factor

$$E(v_r) = \frac{\frac{\pi\alpha_d\xi}{v_r}}{1 - e^{-\pi\alpha_d\xi/v_r}}, \quad (6)$$

where v_r is the *relative* velocity of the scattering particles, and ξ depends on the quadratic Casimir operators of the single-particle representations r_1 and r_2 and the total representation r ,

$$\xi = -\frac{1}{4}(C_2(r) - C_2(r_1) - C_2(r_2)). \quad (7)$$

The annihilation cross-section during freeze-out is then multiplied by the factor

$$E_{ann}(v_r; \{r\}) = \frac{1}{\dim(r_1)\dim(r_2)} \sum_i \dim(r_i) E_i(v_r), \quad (8)$$

which enhances annihilation in attractive channels and exponentially suppresses annihilation in repulsive channels.

As the gluinos are identical particles, we need to ensure that the total wave function is antisymmetric. Annihilation proceeds dominantly in the s -wave, where the wave function is spatially symmetric, and therefore the net color and spin wave function must be antisymmetric. Thus for $N = 2$, the total enhancement factor $E(v)$ is explicitly

$$E(v_r) = \frac{1}{15} \left(\frac{\frac{\pi\alpha_d}{v_r}}{1 - e^{-\pi\alpha_d/v_r}} + 9 \frac{\frac{\pi\alpha_d}{2v_r}}{1 - e^{-\pi\alpha_d/2v_r}} - 5 \frac{\frac{\pi\alpha_d}{2v_r}}{1 - e^{\pi\alpha_d/2v_r}} \right) \quad (9)$$

Incorporating the Sommerfeld enhancement has an order 30% effect on the mass of the dark matter particle relative to perturbative freezeout, as demonstrated in figure 3.

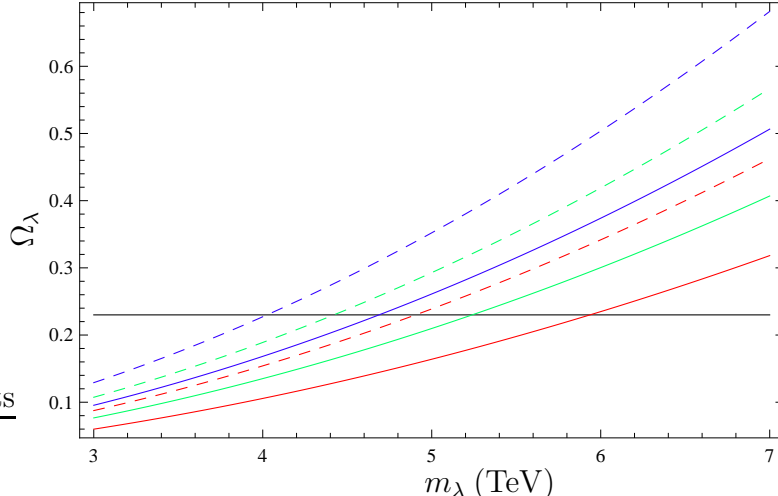


Figure 3: Relic density Ω_λ as a function of m_λ , with (dashed) and without (solid) Sommerfeld enhancement, for $N = 2$. The solid line indicates $\Omega_\lambda = .23$. Relic densities are shown for $m_\lambda/\Lambda = 0.5 \times 10^3$ (red), $m_\lambda/\Lambda = 1 \times 10^3$ (green), and $m_\lambda/\Lambda = 2 \times 10^3$ (blue).

More difficult to estimate are the effects of the increased annihilation cross-sections after confinement, when the λ^a have hadronized [10, 11, 14]. The heavy fermion λ is localized within a region of order its de Broglie wavelength, $1/(m_\lambda v)$, while the total radius of the glueballino is of order $1/\Lambda$. While the *total* interaction cross-section between hadronized adjoints should be geometric, $\sigma_{tot} \sim \pi/\Lambda^2$, the annihilation cross-section should be significantly smaller. Estimating the annihilation cross-section is a subtle problem. The core of the question is whether or not two hadronized λ 's in a state with large angular momentum are kinematically able to radiate away that angular momentum and annihilate. Our hidden sector model differs from QCD in that there are no light fundamental quarks, and hence the mass gap in our hidden sector is larger compared to the strong coupling scale than the mass gap in QCD. We expect that this suppresses the annihilation cross-section in this model, relative to (e.g.) gluino freezeout, as the larger mass gap makes it more difficult to radiate away angular momentum.

We therefore model the late-time annihilation cross-section by taking it to saturate the s -wave unitarity bound,

$$\sigma_{NP} \approx \frac{16\pi}{m_\lambda^2 v_r^2}. \quad (10)$$

We expect that this estimate gives an upper bound on the cross-section, and therefore a lower bound on the relic abundance. This cross-section yields efficient annihilation of hadronized adjoints, lowering the relic density by roughly an order of magnitude relative to the perturbative result. It is therefore difficult to obtain the relic abundance $\Omega_\lambda = 0.23$ without going to corners of parameter space, either large N or m , or small Λ .

As we will explain in the following section, the most interesting choice of dark matter masses from the point of view of neutrino signals is the range 1–5 TeV. This range is consistent with the perturbative computation of the relic abundance. However, if the non-perturbative effects enhancing the annihilation cross-section are close to our estimate (10), this mass range requires either sub-GeV Λ or a very large ($N > 20$) number of dark colors. Building a complete model of the dark sector with Λ significantly less than a GeV requires some additional structure in the dark sector to be consistent with all cosmological constraints, as we discuss in section 5.

4 Dark Matter Decay

The low-energy lagrangian that governs the hidden sector has an accidental \mathbb{Z}_2 symmetry acting as $\lambda \rightarrow -\lambda$ which ensures stability of dark matter. However, general interaction terms do not have to respect this \mathbb{Z}_2 and may lead to dark matter decay. In this section we consider the coupling of dark matter to the standard model via the neutrino portal and study possible decay channels.

The operator $\lambda^a \sigma^{\mu\nu} G_{\mu\nu}^a$ transforms as a fermion under the Lorentz group and as a singlet under both the dark and the standard model gauge groups. Therefore it has the right quantum numbers to couple to the standard model through the neutrino portal. The interaction takes the form

$$\mathcal{L}_{int} = \frac{c}{\Lambda_N^2} \lambda^a \sigma^{\mu\nu} G_{\mu\nu}^a H L + \text{h.c.} \quad (11)$$

Here L is a left-handed weak $SU(2)$ lepton doublet; for definiteness let us assume that it is the first generation doublet, $L = (\nu_L, e_L)$, while the couplings to the second and third generations are suppressed by a larger scale. From the point of view of neutrino detection it does not matter which generation has the dominant coupling to dark matter: the neutrino oscillations will make sure that all 3 neutrino flavors are equally populated in the neutrino flux from dark matter decay.

The interaction (11) breaks the accidental \mathbb{Z}_2 λ -parity and allows the dark matter to decay. It is a dimension six non-renormalizable operator, but it can be easily obtained from a renormalizable UV theory as follows. Let us introduce right-handed neutrinos N_i which have the usual Standard Model couplings. In addition, introduce a pair of fundamentals in the hidden sector: a scalar Q and a (Dirac) fermion χ , which have masses equal to Λ_N . The lagrangian

$$\mathcal{L} = \mathcal{L}_{kin} - \lambda^a (Q^\dagger t^a \chi) - c_i Q^\dagger \chi N_i - Q^\dagger Q |H|^2 - Y_{ij}^N N_i H L_j + \text{h.c.} \quad (12)$$

contains the most general gauge-invariant renormalizable operators which can be built from the fields in the model. Integrating out the heavy Q , χ , and N_i at one loop gives the effective interactions

$$\mathcal{L}_{int} = \frac{c}{\Lambda_N^2} \lambda^a \sigma^{\mu\nu} G_{\mu\nu}^a H L_L + \frac{c_2 m_\lambda}{\Lambda_N^2} \lambda^a \lambda^a |H|^2 + \frac{c_3}{\Lambda_N^2} G_{\mu\nu}^a G^{a\mu\nu} |H|^2 + \text{h.c.} \quad (13)$$

The coefficients c , c_2 , and c_3 are of order $1/16\pi^2$. The latter two interactions have negligible effect on phenomenology, but the first is the desired coupling of dark matter to the standard model via the neutrino portal. If the scale Λ_N is of order $10^{14} - 10^{15}$ GeV—the typical scale for lepton number violating interactions—then the dark matter lifetime is of order 10^{25} seconds. Such a dark matter particle is stable on cosmological time scales and, at the same time, the decay rate may be large enough to allow for detection of dark matter decay products.

The perturbative vertex given by (11) yields two distinct partonic contributions to dark matter decay: first, the $1 \rightarrow 3$ process $\lambda \rightarrow g H L$ with a (hidden) gluon in the final state, and second, the $2 \rightarrow 2$ process $\lambda g \rightarrow H L$, with a (hidden) gluon in the initial state. Both partonic processes are part of the full gauge invariant amplitude for the decay of the dark matter particle, but, as we will see, the first process is the dominant contribution. The main contribution to dark matter decay is then the decay of the heavy adjoint λ^a via (11) to two-body and three-body final states with a hidden gluon plus standard model neutrinos, gauge and Higgs bosons. The hard gluon g from the perturbative decay and the remnants of the brown muck that made up the glueballino go on to hadronize into some number of hidden glueballs.

We first consider the two-body decay with one neutrino and one dark gluon in the final state. The interaction vertex is obtained from (11) by replacing the Higgs field by its vacuum expectation value. The partial decay width is given by

$$\Gamma(\lambda \rightarrow g\nu) \equiv \Gamma_{2b} = \frac{c^2}{32\pi} \frac{m_\lambda^3 v^2}{\Lambda_N^4}. \quad (14)$$

The CP conjugate decay to anti-neutrinos has the same decay width.

Next, consider the three-body decay to gluon, neutrino, and on-shell Higgs boson. The partial width for this process is

$$\Gamma(\lambda \rightarrow gh\nu) = \frac{c^2}{(16\pi)^3} \frac{m_\lambda^5}{\Lambda_N^4} \frac{1}{3} (3 + 44r - 36r^2 - 12r^3 + r^4 + 12r(2 + 3r) \ln r), \quad (15)$$

where $r = m_h^2/m_\lambda^2 \ll 1$. Again, the CP conjugate decay to anti-neutrinos occurs with the same rate. In the limit $r \rightarrow 0$

$$\Gamma(\lambda \rightarrow gh\nu) = \Gamma(\lambda \rightarrow gh\bar{\nu}) \approx \frac{c^2}{(16\pi)^3} \frac{m_\lambda^5}{\Lambda_N^4} \equiv \Gamma_{3b}. \quad (16)$$

In addition, there are three-body decay modes to (i) gluon, electron, and W boson; (ii) gluon, neutrino and Z boson. In the limit $m_{W,Z}/m_\lambda \rightarrow 0$ these partial widths satisfy the relation

$$\Gamma(\lambda \rightarrow gZ\nu) = \Gamma(\lambda \rightarrow gZ\bar{\nu}) = \frac{1}{2}\Gamma(\lambda \rightarrow gW^+e^-) = \frac{1}{2}\Gamma(\lambda \rightarrow gW^-e^+) = \Gamma_{3b} \quad (17)$$

Ignoring gauge and Higgs masses, the dark matter lifetime is approximately

$$\tau_\lambda \approx \frac{1}{2(\Gamma_{2b} + 4\Gamma_{3b})}, \quad (18)$$

while the ratio of two- and three-body partial widths is

$$\frac{\Gamma_{3b}}{\Gamma_{2b}} \approx \frac{1}{128\pi^2} \frac{m_\lambda^2}{v^2} \approx 0.01 \left(\frac{m_\lambda}{\text{TeV}} \right)^2 \quad (19)$$

Varying m_λ in the range 1-5 TeV, the three-to-two-body ratio varies from 1 percent to 30 percent. Therefore the neutrino flux from dark matter decay dominates over charged particle fluxes, especially when the glueballino is not much heavier than 1 TeV.

Apart from the process where the adjoint fermion decays into a dark gluon and standard model fields one can also consider the annihilation of the fermion with a valence gluon. We argue however that this gives a negligible contribution to glueballino decay. First, it is readily apparent that the rate for the gluino to completely annihilate with its cloud of gluons is vanishingly small. In order for the glueballino to annihilate into the vacuum, all of the momentum distributed among the brown muck must be concentrated in a single partonic gluon which then annihilates with the heavy fermion λ , or in other words, all of the momentum carried by the gluons must be entirely localized within the Compton wavelength of the heavy fermion λ . The probability for this to occur is negligibly small, of order $(\Lambda/m_\lambda)^3$ at most. Moreover, the probability for the operator $\lambda^a \sigma^{\mu\nu} G_{\mu\nu}^a$ to connect the initial state glueballino to a single glueball at rest is suppressed. This process can be thought of as an annihilation of the partonic λ^a with a coherent sum of soft gluons inside the hadron. The residual soft gluons after annihilation must carry enough energy to reform into a stable glueball. As the glueballs have masses of a factor of a several larger than the strong coupling scale, an annihilation of this form is kinematically forbidden unless the λ^a has a virtuality likewise several times larger than the strong coupling scale. Computing the cross-section for $\lambda^a + g \rightarrow h\nu$ and taking $p_g \sim \Lambda$, we can estimate

$$\sigma \sim \frac{c^2}{\Lambda_N^4} \frac{m_\lambda \Lambda (1-r)^2}{24\pi}. \quad (20)$$

Strictly, as the gluon participating in the interaction is soft we need to integrate this expression over the field configuration of the glueballino. To obtain an estimate for the

annihilation rate we simply estimate the result of this integral as Λ . This yields an estimate for the rate

$$\Gamma \sim \frac{c^2}{\Lambda_N^4} \frac{m_\lambda \Lambda^2 (1-r)^2}{24\pi} : \quad (21)$$

this is suppressed relative to the two-body decay rate (14) by a factor of $(\Lambda/v)^2$. However the rate for the full process should be suppressed even further, as the gluino must have emitted a hard gluon before participating in the annihilation in order to be sufficiently off-shell. This emission suppresses the annihilation process by an additional factor of α_d . In the following, we will neglect this glueballino decay mode in comparison with the two- and three-body decay modes coming from the decay of the gluino alone.

5 Interlude: Glueball Decays

The hidden sector glueballs cannot be stable on cosmological time scales as otherwise they would overclose the universe. In this section we discuss the thermal relic abundance of glueballs and present several scenarios for their decay. We will show that there are multiple ways to eliminate the overabundance of glueballs, and will indicate the observable signals associated with each scenario. At the end of the day it will be clear that the signals and resulting constraints are very model-dependent, in contrast to the sharp predictions from two- and three-body decays via the neutrino portal discussed in Section 4. Therefore, when discussing signals and constraints in the following of this paper we will focus on the more robust signals of the standard model particles coming directly from the neutrino portal operator $\lambda^a G_{\mu\nu}^a \sigma^{\mu\nu} H L$. The goal of this section is to point out and characterize a range of options for addressing the glueball problem, and demonstrate that solutions are possible. Readers less interested in model building and more interested in model-independent astrophysical signatures of the neutrino portal are encouraged to jump directly to the next section.

First, we demonstrate why the glueballs must decay. Treating hidden sector confinement as adiabatic, the energy and entropy in the thermal gluon bath are wholly transferred to glueballs after confinement. If the glueballs do not decay, the present-day energy density in glueballs is then given in terms of the present-day photon temperature T_0 by

$$\rho_{glue}(t_0) \approx \frac{\pi^2}{30} \Lambda T_0^3 \frac{g_{*0} g_{*D}}{g_{*SM}}, \quad (22)$$

where $g_{*,0}$ is the effective number of relativistic standard model degrees of freedom today, and $g_{*,D,SM}$ are the effective number of relativistic degrees of freedom in the dark sector and in the standard model when the two sectors were in thermal equilibrium. Avoiding

overclosure then requires the strong coupling scale Λ to be smaller than an eV,

$$(N^2 - 1) \frac{\Lambda}{\text{eV}} \lesssim 1. \quad (23)$$

However, the strong coupling scale Λ is constrained by astrophysical bounds on the dark matter self-interaction cross-section. Analyses of galactic cluster dynamics combine to yield a bound on the total dark matter self-interaction cross-section [16, 17, 18, 19],

$$\frac{\sigma}{m} \lesssim 0.3 - 1 \text{ cm}^2 \text{g}^{-1} \approx 1400 - 4600 \text{ GeV}^{-3}. \quad (24)$$

The most stringent such astrophysical bound comes from observations of the Bullet Cluster, 1E0657-56 [18, 19]. In our model, the *total* self-interaction cross-section for the glueballino is geometric, $\sigma_{tot} \sim \pi/\Lambda^2$. With $\Lambda \sim \text{eV}$, the bound (24) requires the mass of the glueballino to be very large, $m_\lambda \gtrsim 10^9 \text{ GeV}$, which would be incompatible with thermal relic abundance.

As the glueball masses are intrinsically tied to the confinement scale, there is no way to escape this problem. The glueballs must therefore decay. There are then three possibilities: the glueballs can decay within their own sector; they can decay to the standard model; or finally, they can decay to yet another sector. Adding light flavors to the hidden sector gauge theory destabilizes the glueballs to hidden sector mesons and opens an interesting range of possibilities for model building, which we discuss below.

Another option, which we will pursue here, is to add additional degrees of freedom (“mediators”) which couple the hidden and visible sector, enabling glueballs to decay to standard model final states. Dark matter decays then yield a model-dependent amount of visible standard model particles from glueball decays in addition to the primary gluino decay, which must be taken into account. In order to avoid cosmological constraints, it is simplest to ask that the lifetime of at least one species of glueball be less than one second, so that the glueballs can safely decay without a trace before nucleosynthesis. For definiteness, we will consider two simple models where the mediators couple to the standard model Higgs boson, thereby enabling the 0^{++} glueball to decay rapidly through the dimension 6 Higgs portal operator to pairs of standard model fermions. In the first model, we introduce a standard model singlet scalar field ϕ transforming as a fundamental under the dark gauge group, with the interaction

$$\mathcal{L}_{int} = y|\phi|^2|H|^2. \quad (25)$$

In the second model, we introduce a pair of Dirac fermions, K_L and P_R , which are fundamentals under the dark gauge group and have the standard model quantum numbers of a left-handed lepton doublet and a right-handed charged lepton, respectively. The interactions of the new fermions K_L and P_R we take to be C - and P -preserving, for simplicity:

$$\mathcal{L} = \mathcal{L}_{kin} + (y\bar{P}_R H K_L + h.c.). \quad (26)$$

Integrating out the mediators induces the dimension six interaction

$$\mathcal{L}_{eff} = \frac{g^2 c}{4\pi^2 M^2} H^\dagger H G_{\mu\nu}^a G^{a\mu\nu}. \quad (27)$$

Here M is the mass scale of the mediators. The coefficient c is $y^2/12$ for the scalar mediator model of equation (25), and $2y^2/3$ for the fermion mediator model of equation (26).

The 0^{++} glueball decays through the effective interaction (27) with branching fractions dictated by the couplings of the standard model Higgs. For the parameter range we consider, the 0^{++} will decay to pairs of standard model fermions through an off-shell Higgs. The width for this decay is given by

$$\Gamma_{0^{++} \rightarrow f\bar{f}} = \left(\frac{cvF_{0^+}^S}{16\pi^2 M^2 (m_h^2 - m_0^2)} \right)^2 \Gamma_{h \rightarrow f\bar{f}}^{SM}(m_0^2) \quad (28)$$

Here $\Gamma_{h \rightarrow f\bar{f}}^{SM}(m_0^2)$ denotes the partial width of $h \rightarrow f\bar{f}$ for a standard model Higgs boson with mass m_0 , and $F_{0^+}^S$ is the 0^{++} decay constant. We will use the lattice result for $F_{0^+}^S$ [20] ,

$$F_0^S \equiv g^2 \langle 0 | G_{\mu\nu}^a G^{a\mu\nu} | 0^{++} \rangle = 6.12 m_0^3. \quad (29)$$

If the 0^{++} is heavy enough to decay to $b\bar{b}$ pairs, a lifetime less than one second is readily accomplished with mediator mass scales in the range of tens to hundreds of TeV. Lighter glueballs, with masses in the range $2m_\tau < m_{0^{++}} < 2m_b$, are also viable if the mediator mass scales are in the range of a few to tens of TeV. Glueballs light enough to decay dominantly to muon pairs are interesting, as this mass range appears best compatible with obtaining the correct relic density for the heavy hadronized adjoint, as well as with possible visible signals. However, realizing a sufficiently short lifetime for the 0^{++} in this case requires the mediators to be so light that they lie outside the range of validity of our calculations. Models with light standard model-charged mediators are ruled out, but a light scalar mixing with the standard model Higgs is entirely possible, and seems like an interesting avenue to pursue.

In the case of a scalar mediator, the only interactions induced upon integrating out the heavy mediators are of the form

$$\mathcal{L}_{eff} = G_{\mu\nu}^a G^{a\mu\nu} \sum_k \frac{c_k}{M^{2+k}} (H^\dagger H)^k. \quad (30)$$

The Lorentz decomposition of the operator $G_{\mu\nu}^a G^{a\mu\nu}$ contains only the 0^{++} . Therefore only the 0^{++} can decay directly via the Higgs portal to standard model particles. Other glueballs can decay through the 0^{++} channel, e.g., $2^{++} \rightarrow (0^{++})^* 0^{++} \rightarrow f\bar{f} 0^{++}$. These three-body decay rates are highly suppressed relative to the 0^{++} decay rate due to the

smaller available phase space. The only glueballs which cannot decay in this manner are the lightest states in the P and C -odd sectors, the 0^{-+} and 1^{+-} . Without explicit P or C violation, no dimension 6 operator permits the 0^{-+} and 1^{+-} states to decay into standard model fermions.

In the case of bifundamental mediators, loops of the heavy particles also induce dimension 8 effective interactions coupling the hidden gluons to standard model gauge bosons,

$$\mathcal{L}_{eff} = c_1 \frac{g_i^2 g_v^2}{M^4} \text{Tr} F_i^2 \text{Tr} G^2 + c_2 \frac{g_1 g_v^3}{M^4} F_1 \text{Tr} G^3, \quad (31)$$

considered in detail in [21] in the context of hidden valley signals at the LHC. Here F (G) is the field strength tensor for standard model (dark sector) gauge fields. The field strength tensors are contracted according to different irreducible representations of the Lorentz group which for the sake of brevity are not shown here. These dimension 8 operators allow all the hidden sector glueballs to decay, either directly to standard model gauge boson pairs (the 0^{++} , 2^{++} , 0^{-+} , 2^{-+}) or radiatively to another glueball via the emission of a photon (all others).

For a glueball which can decay either through radiative photon emission or through an off-shell Higgs, the situation is rather involved. The branching ratios of these two modes depend critically on the mass scale M of the mediators and the nonperturbative transition matrix elements. The ratio of the partial widths can be written parametrically as

$$\frac{\Gamma_{A \rightarrow C\gamma}}{\Gamma_{A \rightarrow Bff}} \approx \left(\frac{m_H}{yM}\right)^4 \left(\frac{m_A}{m_f}\right)^2 \alpha \alpha_d \chi^2 \frac{1}{I\left(\frac{m_B}{m_A}, \frac{m_f}{m_A}\right)} \quad (32)$$

where $\chi = M^4(1/m_K^4 - 1/m_P^4)$ and α is the fine structure constant. The dimensionless phase-space function $I(a, b)$ is given by

$$I(a, b) = \int_{4b^2}^{(1-a)^2} dx x (g(a^2, x; 1))^{L+1/2} (g(b^2, b^2; x))^{3/2}. \quad (33)$$

where $g(x, y; z) = (1 - x/z - y/z)^2 - 4xy/z^2$ and L is the relative orbital angular momentum of A and B . Given the masses in Fig. 1, $I \approx 10^{-6} - 10^{-5}$. For $\chi \sim 0.1 - 0.5$, which is a conservative choice if the mass splittings between the mediator fields are not especially large, the larger suppression of dimension eight operators tends to suppress the radiative decays in favor of the three-body decays. However, for small enough M , the radiative decays can become competitive. Indeed, a simple estimate suggests that for $M \gtrsim 10$ TeV, the dimension 6 operator dominates, while for mediators within the reach of the LHC radiative and three-body rates can be comparable. If the off-shell Higgs needs to decay

to muon pairs, the small muon Yukawa coupling will additionally suppress the three-body rates, making the radiative decays dominate.

To summarize, glueball decays contribute b quarks or τ leptons to the visible signals of dark matter decay, as well as possible photons (both singly and in pairs) if the mediators are charged under $SU(2)_L \times U(1)_Y$. (Decays into W and Z bosons are kinematically impossible.) Colored mediators would also allow the glueballs to decay into standard model gluon pairs, but in order to minimize the antiprotons coming from glueball decays we have taken the mediators to be color singlets. Moreover, as most of the mass splittings between glueballs are smaller than m_0 , if the 0^{++} is near the threshold to decay to $b\bar{b}$ pairs, then kinematics may prevent $b\bar{b}$ pairs from being produced in three body decays of heavier glueballs. A typical final visible state would then be of the form $b\bar{b}c\bar{c}$, $b\bar{b}\tau^+\tau^-$ and so on. A similar story holds for 0^{++} decaying to tau pairs: higher-mass glueballs could yield pion and muon pairs in addition to the tau pairs coming from the decay of the terminal 0^{++} . Glueballs which decay mainly into muon or pion pairs might be obtained with additional model building in the Higgs sector.

While it is possible to work out glueball branching fractions for a given mediation model with the help of lattice data for $N = 3$, it is considerably more difficult to arrive at the full spectrum of visible standard model particles produced in a single glueballino decay. The injection spectrum dN_{SM}/dE of visible standard model particles depends on the number and spectra of glueballs initially produced in the glueballino decay. In order to make crisp predictions about indirect detection signals coming from dark matter decay, we therefore need to understand the process of fragmentation in pure Yang-Mills theory. Unfortunately, this is a situation where neither phenomenological examples from QCD nor data from the lattice can be of help. In the absence of light fundamentals, the color tube connecting hard partons cannot break. Glueball formation in a pure Yang-Mills theory occurs heuristically through the crossing of the tube onto itself, a process qualitatively different from fragmentation in QCD.

One simple approach to estimating the relative abundances of different glueball species is a thermal model. In such a model, the ratio of the multiplicity of glueballs is given by

$$\frac{N_J}{N_0} = (2J + 1) \left(\frac{m_J}{m_0} \right)^{3/2} \exp^{-(m_J - m_0)/T} \quad (34)$$

where m_J (N_J) is the mass (multiplicity) of a glueball with spin J . The effective temperature T can be taken as the center of mass energy of the colored system immediately following the decay of the heavy adjoint fermion, $T \sim \sqrt{\Lambda m_\lambda}$. With $m_\lambda \gg \Lambda$, the thermal model predicts glueball democracy in the final state: for $m_\lambda = 1 \text{ TeV}$ and $\Lambda = 1 \text{ GeV}$, the heaviest of the stable glueballs, the 0^{+-} , is produced two-thirds as frequently as the

0^{++} . Unfortunately, the applicability of the thermal model to pure Yang-Mills theory is unclear. In particular, excitations of the flux tube (such as can easily be produced from gluon showering in the final state) might enhance the production of the higher-spin states above the thermal estimate. Moreover, the thermal model is not well-suited to address a key question for indirect detection: what is the average *total* number of glueballs per decay?

To arrive at an injection spectrum dN_{SM}/dE which can be compared to indirect detection data, we need to specify not only a particular model for glueball decay but also a model for fragmentation in the hidden sector. While it appears possible to build interesting models which have the potential to avoid overproduction of antiprotons, it is clear that not only is there significant freedom in the detailed choice of model, but also that a reasonable model of pure-gluon fragmentation is a necessary ingredient in quantifying the predictions of such models for indirect detection experiments.

5.1 Model Building with Light Hidden Flavor

Adding light ($m_q \lesssim \Lambda$) fundamental flavors to the hidden sector destabilizes the glueballs to hidden mesons, without destabilizing the adjoint fermion λ . As λ is fermionic, it must decay to an odd number of hidden quarks and anti-quarks. But such a final state carries non-zero hidden-sector baryon number. The decay of λ to light flavor therefore violates baryon number, and is therefore forbidden in the absence of hidden sector baryon number violation.

The meson masses depend on the input light quark masses as well as on the strong coupling scale, and can be tuned independently of the other parameters of the theory. Avoiding overclosure requires that the hidden mesons have sub-eV masses, giving rise to a large but technically natural hierarchy, $m_q \ll \Lambda \ll m_\lambda$. However, the existence of such extremely light mesons leads to concerns that inelastic glueballino scattering $\Psi\Psi \rightarrow \Psi\Psi + n\pi_v$ may exceed observational bounds on dissipative dark matter interactions. Adding such extremely light mesons will also dramatically increase the late-time glueballino annihilation cross-section, likely to a problematic extent.

More attractive model building possibilities are realized by keeping $m_q \sim \Lambda$ and allowing the hidden sector mesons to decay to the standard model. This can be realized in multiple ways. One option is to introduce a Z' coupling to both hidden flavor and visible standard model fermions [7]. This allows at least one hidden sector meson to decay to a pair of standard model fermions, with a preference for heavier fermions due to helicity suppression. The main challenge is then obtaining a short enough lifetime for the shortest-lived hidden sector meson while keeping $m_q \sim \Lambda \sim m_{\pi_v}$ at the GeV scale. For models of the form considered in [7], lifetimes of less than a second can be achieved for $2m_\tau < m_q \sim \Lambda$, with

the mediator mass in the range of a few to tens of TeV. Decay to muon pairs can only be realized for a light mediator and m_{π_ν} close to the τ threshold.

Models with light flavor have one especially nice feature: they allow for more concrete predictions for the visible signals from dark matter decay, as with the addition of light flavor it is possible to adapt models of fragmentation in QCD. This then allows definite predictions for the spectra and multiplicities of the hidden sector hadrons produced in dark matter decay, which in turn allows detailed comparison to astrophysical data. While this is appealing, it comes at a cost: the existence of light degrees of freedom in the hidden sector exacerbates the uncertainties in evaluating the annihilation cross-section for glueballinos, and hence in the acceptable mass range for the dark matter. Nonetheless, there are interesting avenues for model building here.

6 Constraints from indirect detection

We turn to discussing the constraints on our neutrino portal scenario from various indirect detection experiments. The glueballino decaying via the operator of Eq. (2) produces dominantly neutrinos, but also Higgs particles, W and Z bosons, and electrons and positrons. These fluxes of standard model particles produced directly from the neutrino portal operator are relatively model-independent: the relative normalization of the two- and three-body decay modes depends only on the kinematics of the decay. Bounds on these decay modes therefore constrain the general scenario where structure in the dark sector enables dark matter decaying through the neutrino portal to yield a primary flux of monochromatic neutrinos. We compute the fluxes of neutrinos, antiprotons, positrons, and gamma rays observed at the Earth for standard model particles produced in the decay of the heavy dark matter particle, and determine the allowed parameter space of our model.

Throughout this section we assume the dark matter distribution in our galaxy is described by the Einasto profile

$$\rho_{DM}(r) = \rho_0 \exp \left[-2 \frac{(r/r_s)^\alpha - 1}{\alpha} \right] \quad (35)$$

where r is the distance from the center of our galaxy, and we use the values $\alpha = 0.17$ and $r_s = 20$ kpc [22]. The normalization constant is $\rho_0 = 0.06 \text{ GeV/cm}^3$ which gives the local dark matter energy density $\rho_\odot \equiv \rho_{DM}(r_\odot) = 0.3 \text{ GeV/cm}^3$. Here $r_\odot = 8.5$ kpc is the distance of the Solar System from the galactic center. Because for decaying dark matter the signal depends on ρ_{DM} (rather than ρ_{DM}^2 as for annihilation) there is limited sensitivity

to the choice of the profile. For example, another standard profile, the NFW profile

$$\rho_{DM}(r) = \rho_0 \left(\frac{r_s}{r}\right)^\gamma \left(1 + \left(\frac{r}{r_s}\right)^\alpha\right)^{(\gamma-\beta)/\alpha} \quad (36)$$

with parameter choices $\{\alpha, \beta, \gamma\} = \{1, 3, 1\}$, $r_s = 20$ kpc, and $\rho_0 = 0.26$ GeV/cm³ [23], increases the neutrino flux above that predicted using the Einasto profile by about 10 percent.

6.1 Neutrino bounds from Super-Kamiokande

Dark matter decaying in our galaxy produces mostly neutrinos and antineutrinos with energy equal to $m_\lambda/2$. This leads to a flux of cosmic neutrinos concentrated in the direction toward the galactic center. The interaction cross-sections of dark matter with nuclei in our model are negligible, leading to correspondingly negligible dark matter capture rates in the Earth and the Sun. Therefore only bounds on neutrino flux from the galactic center are constraining. To date, the best bounds on such a flux are those from the Super-Kamiokande collaboration [24, 25].

The flux of neutrinos coming from dark matter decay is given by

$$\frac{d\Phi_\nu}{dE_\nu d\Omega}(m_\lambda) = \frac{1}{4\pi} \frac{\Gamma_\lambda}{m_\lambda} \frac{dN}{dE_\nu} \int ds \rho(s), \quad (37)$$

where dN/dE_ν is the spectrum of neutrinos generated in the dark matter decay, and the integral of the dark matter energy density is taken along a line of sight. It is conventional to define the dimensionless quantity

$$\frac{dJ}{d\Omega} = \int \frac{ds \rho(s)}{r_\odot \rho_\odot}, \quad (38)$$

normalizing the line of sight density integral to our local position and density. The flux in a cone of half-angle ψ around the galactic center is then

$$\frac{d\Phi_\nu}{dE_\nu}(m_\lambda; \psi) = \frac{1}{4\pi} \frac{\Gamma_\lambda}{m_\lambda} \frac{dN}{dE_\nu} r_\odot \rho_\odot \times \Delta J(\psi), \quad (39)$$

with

$$\Delta J(\psi) = \frac{2\pi}{r_\odot \rho_\odot} \int_{\cos \psi}^1 d \cos \theta \int_0^{r_0} dx \rho(\sqrt{r_\odot^2 + x^2 - 2r_\odot x \cos \theta}). \quad (40)$$

Notice that Eq. (39) is the total neutrino flux, summed over all three flavors, as oscillation over galactic scales will equally populate all three flavors. Moreover, there is an equal in magnitude anti-neutrino flux.

Having fixed the halo profile in Eq. (35), ΔJ is a function of the half-cone angle which can be computed numerically. Neutrinos produced in a decay travel to the Earth without experiencing further interactions. The normalization of the neutrino flux at the Earth depends on the dark matter lifetime and mass via the ratio Γ_{2b}/m_λ , and this is the quantity that will be constrained by Super-Kamiokande.

The published Super-Kamiokande bounds do not apply directly to the neutrino flux but rather to the upward-going muon flux. These muons are produced by charged current interactions of the cosmic neutrinos in the rock below the detector. In order to translate the neutrino and antineutrino fluxes into a muon flux we need to compute the conversion functions $C_{\nu \rightarrow \mu^-}(E_\mu; E_\nu)$ and $C_{\bar{\nu} \rightarrow \mu^+}(E_\mu; E_\nu)$,

$$\frac{d\Phi_{\mu^-}}{dE_\mu} = \int dE_\nu \frac{dC_{\nu \rightarrow \mu^-}}{dE_\nu} \frac{d\Phi_\nu}{dE_\nu}, \quad \frac{d\Phi_{\mu^+}}{dE_\mu} = \int dE_\nu \frac{dC_{\bar{\nu} \rightarrow \mu^+}}{dE_\nu} \frac{d\Phi_{\bar{\nu}}}{dE_\nu}. \quad (41)$$

which encapsulate the probability that a neutrino will interact in rock to produce a muon of energy E_μ which reaches the detector. The conversion functions depend on the muon range in rock $R_\mu(E_\mu)$, the proton and neutron number densities in rock n_N , $N = n, p$, and the neutrino inelastic scattering cross section on nucleons $\sigma_{\nu N}$:

$$\frac{dC_{\nu \rightarrow \mu^-}}{dE_\mu} = R_\mu(E_\mu) \left[n_p \frac{d\sigma_{\nu p}}{dE_\mu} + n_n \frac{d\sigma_{\nu n}}{dE_\mu} \right], \quad \frac{dC_{\bar{\nu} \rightarrow \mu^+}}{dE_\mu} = R_\mu(E_\mu) \left[n_p \frac{d\sigma_{\bar{\nu} p}}{dE_\mu} + n_n \frac{d\sigma_{\bar{\nu} n}}{dE_\mu} \right]. \quad (42)$$

To compute the neutrino-nucleon scattering cross sections, we use the tree-level partonic cross-section integrated over the CTEQ5 parton distribution functions. We perform our computations using the fiducial material “standard rock”, for which the nucleon densities are $n_p = n_n \approx 6.1 \times 10^{-18} \text{ GeV}^3$.

The last piece we need to evaluate Eq. (42) is the muon range $R_\mu(E_\mu)$, the distance a muon with the initial energy E_μ can travel before its energy is radiated away so as to fall below the Super-Kamiokande threshold $E_0 = 1.6 \text{ GeV}$. The muon range can be modeled analytically using the “continuous slowing down approximation”, with parameters found in [26]. We approximate the muon range $R_\mu(E_\mu)$ as

$$R_\mu(E_\mu) \approx 10^5 \text{ cm} \ln \left(\frac{E_\mu + \epsilon}{\epsilon} \right), \quad (43)$$

Here ϵ is the critical energy, where ionization and radiation loss are equal; we take ϵ to be 693 GeV in standard rock [26] (we assume that cross sections in standard rock are comparable to cross sections in the rock below Super-Kamiokande). The continuous slowing down approximation becomes poor at high energies, where stochastic radiative processes dominate the energy loss. More accurate Monte Carlo modeling of muon propagation

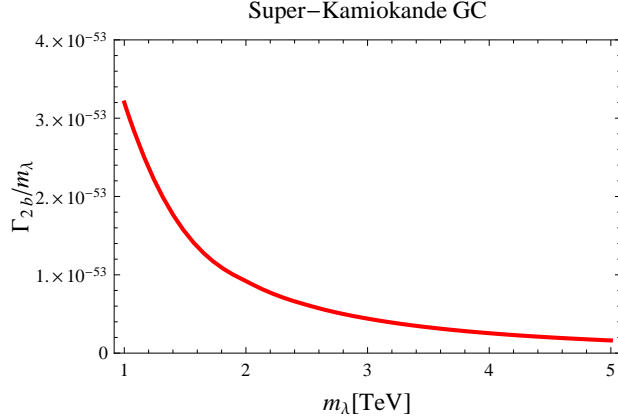


Figure 4: The maximal Γ_{2b}/m_λ as a function of m_λ allowed by the Super-Kamiokande bounds.

at high energies reduces the flux of upward-going neutrino-induced muons at neutrino detectors for a given incident neutrino flux relative to the flux obtained using the continuous slowing down approximation [27]. Comparing the effective muon range given by (43) to the effective muon range computed in [27] for muons with energy $> \text{TeV}$, we find our muon ranges are overestimated by a factor of less than order unity over most of the energy range. The bounds we obtain from Super-Kamiokande’s reported upward through-going muon counts are therefore conservative.

Finally, to obtain the total muon flux in the Super-Kamiokande detector we have to integrate over all muon energies between E_0 and $m_\lambda/2$. At the end of the day the muon flux in Super-Kamiokande is given by

$$\Phi_{\mu^\pm}(\psi) = \frac{1}{3} \frac{\Gamma_{2b}}{m_\lambda} \frac{r_\odot \rho_\odot}{4\pi} \Delta J_{ls}(\psi) \int_{E_0}^{m_\lambda/2} dE_\mu \left[\frac{dC_{\nu \rightarrow \mu^-}}{dE_\mu} + \frac{dC_{\bar{\nu} \rightarrow \mu^+}}{dE_\mu} \right] \quad (44)$$

The factor $1/3$ arises because $2/3$ of the produced neutrinos oscillate into electron and tau neutrinos to which Super-Kamiokande is far less sensitive.

The muon flux induced by neutrinos from the galactic center predicted by our model is dominated by the monoenergetic neutrinos from the dominant two-body decay. At higher dark matter masses, $m_\lambda \sim 5 \text{ TeV}$, the additional neutrinos from the sub-dominant three-body modes begin to make a noticeable contribution to the total muon flux. We computed the total muon flux predicted from our model and confronted it with the Super-Kamiokande bounds from [24]. The most stringent bounds are obtained for cones of half-angle 30 degrees. In Fig. 4 the resulting bound on Γ_{2b}/m_λ is plotted as a function of m_λ . The dark matter mass is varied in the range $1 - 5 \text{ TeV}$, as motivated by the estimate of thermal abundance

in the previous section. For $m_\lambda = 1$ TeV the bound is $\Gamma_{2b}/m_\lambda \lesssim 3.2 \times 10^{-53}$, corresponding to the lifetime $\tau \approx 9.9 \times 10^{24}$ seconds. For $m_\lambda = 5$ TeV the bound is $\Gamma_{2b}/m_\lambda \lesssim 1.6 \times 10^{-54}$, corresponding to the lifetime $\sim 1.9 \times 10^{25}$ seconds.

The sub-dominant three-body decays lead to additional visible signals, in particular, to antiprotons, hard leptons (which we take here as e^\pm), and photons. In the following subsections we investigate the predicted antiproton, positron and gamma ray fluxes arising from the three-body decay modes to determine whether these subleading decays impose more stringent bounds on the lifetime of our dark matter particle than the two-body decays.

6.2 Antiproton bounds from PAMELA

An irreducible source of antiprotons in our model are the decays of the W , Z , and Higgs bosons which are produced by the three-body decays of our dark matter particle. On average, these channels lead to one energetic antiproton per decay. The branching ratio for three-body decays varies from 4 percent of the total width for $m_\lambda = 1$ TeV to as much as 55 percent for $m_\lambda = 5$ TeV. Thus we expect that the antiproton bounds on the dark matter lifetime can become quite stringent in some regions of the parameter space.

The production rate of antiprotons per unit energy due to the three-body decays is given by

$$Q_{\bar{p}}(E, \vec{r}) = 2 \frac{\Gamma_{3b}}{m_\lambda} \rho_{DM}(\vec{r}) \left(\frac{dN_{Z \rightarrow \bar{p}}}{dE} + \frac{dN_{h \rightarrow \bar{p}}}{dE} + 2 \frac{dN_{W \rightarrow \bar{p}}}{dE} \right). \quad (45)$$

We determined the antiproton spectra $dN_{\rightarrow \bar{p}}/dE$ by first generating W , Z , and Higgs decays at rest using Pythia 6.420, and then boosting the momenta of antiprotons to the galactic rest frame. The energy distribution of the parent gauge and Higgs bosons is given by the differential decay width, which is the same for all three particles in the limit $m_\lambda \gg m_{h,W,Z}$:

$$\frac{1}{\Gamma_{3b}} \frac{d\Gamma_{3b}}{dE} = \frac{32}{m_\lambda^4} E(m_\lambda - 2E)(m_\lambda - E). \quad (46)$$

Throughout, the Higgs is assumed to have standard model properties and the mass equal 115 GeV.

In order to translate the production rate into the flux of antiprotons at the Earth it is necessary to model the propagation of antiprotons in our galaxy [28]. The antiproton number density per unit energy $N_{\bar{p}}$ satisfies a diffusion equation

$$K(E) \nabla^2 N_{\bar{p}}(E, \vec{r}) - \partial_z (V_c \text{sgn}(z) N_{\bar{p}}(E, \vec{r})) - 2h\delta(z) \Gamma_{ann}(E) N_{\bar{p}}(E, \vec{r}) + Q_{\bar{p}}(E, \vec{r}) = 0 \quad (47)$$

in which the production rate (45) appears as the source term. Energy loss for protons is negligible and the corresponding term in the diffusion equation is dropped. The diffusion

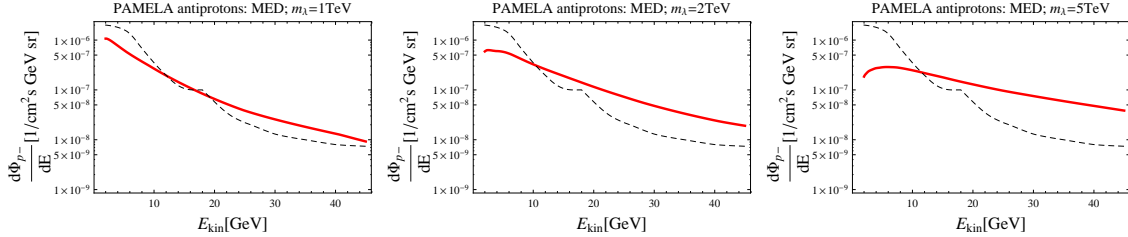


Figure 5: Antiproton flux from the three-body decay of the gauginos (solid red) compared to the flux measured by PAMELA (dashed) for dark matter masses $m_\lambda = 1, 2,$ and 5 TeV. In each case the glueballino decay rate is set to the maximal value allowed by the Super-Kamiokande bounds.

coefficient $K(E)$ is parameterized as $K(E) = K_0(E/\text{GeV})^\delta$. The parameters K_0 and δ are not known from first principles; instead, they are fitted, along with the magnitude of the convective wind V_c and the size of the diffusion zone, so as to correctly describe the observed flux of cosmic rays. The third term describes the disappearance of antiprotons due to annihilations with protons in the galactic disk. The half-height of the galactic disk is set by $h = 0.1$ kpc, and the annihilation width is given by the number densities of hydrogen and helium multiplied by the proton-antiproton annihilation cross-section, $\Gamma_{ann}(E) = (n_H + 4^{2/3}n_{He})\sigma_{p\bar{p}}(E)$. Expressions for n_H, n_{He} and the proton-antiproton annihilation cross-section $\sigma_{p\bar{p}}(E)$ can be found in [29]. The diffusion equation Eq. (47) is solved subject to the boundary condition that the antiproton density $N_{\bar{p}}$ vanish at the surface of the diffusion region, taken to be a cylinder of radius $R_{max} = 20$ kpc and half-height L_{max} .

In the following we focus on the MED propagation model [30], in which case the diffusion equation parameters take the following values:

$$K(E) = 3.5 \times 10^{-10} \text{kpc}^2/\text{s}; \quad \delta = 0.7; \quad V_c = 1.2 \times 10^6 \text{cm/s}; \quad L_{max} = 4 \text{kpc}. \quad (48)$$

Once we know $N_{\bar{p}}$, the flux of antiprotons observed at the Earth is given by $\frac{d\Phi_{\bar{p}}}{dE} = \frac{v}{4\pi} N_{\bar{p}}(E, \vec{r}_\odot)$; in the interesting energy range the antiprotons are highly relativistic and $v \approx 1$.

The propagation equation can be solved semi-analytically [31]. Using that solution, the antiproton flux in our model is given by

$$\frac{d\Phi_{\bar{p}}}{dE} = \frac{1}{2\pi} \frac{\Gamma_{3b}}{m_\lambda} \left(\frac{dN_{Z \rightarrow \bar{p}}}{dE} + \frac{dN_{h \rightarrow \bar{p}}}{dE} + 2 \frac{dN_{W \rightarrow \bar{p}}}{dE} \right) \rho_{DM}(r_\odot) R(E). \quad (49)$$

The propagation effects are encoded in the function $R(E)$ which can be computed numerically [31, 30].

With this solution in hand we are ready to estimate the antiproton constraints on the lifetime of our dark matter particle. We pick three representative values for the dark matter mass: $m_\lambda = 1, 2, 5$ TeV. For the sake of comparison with the neutrino bounds, for each mass we choose the maximum Γ_{2b}/m_λ allowed by Super-Kamiokande as plotted in Fig. 4. Given Γ_{2b} and m_λ , the partial width for three-body decays Γ_{3b} is completely determined by equation (19). The mass fixes the spectra dN/dE , while the partial width fixes the normalization of the antiproton flux in Eq. (49). Our results are plotted in Fig. 5 and compared to the antiproton flux measured by PAMELA. It is clear that antiprotons, despite being produced by subdominant decay channels, can put important constraints on the dark matter lifetime. For $m_\lambda = 5$ TeV, the predicted antiproton flux is 5 times larger than observed, which would imply the stringent bound $\Gamma_{2b}/m_\lambda \lesssim 3 \times 10^{-55}$ corresponding to the lifetime $\sim 10^{26}$ sec. For $m_\lambda = 1$ TeV, the predicted antiproton flux is only marginally larger than observed, and is slightly more constraining than the Super-Kamiokande bound. One should however keep in mind that the propagation of antiprotons in our galaxy suffers from huge uncertainties, and the predicted antiproton flux changes dramatically with different assumptions about the propagation model. For example, choosing the MIN parameters for the propagation model [30],

$$K_0 = 5.1 \times 10^{-11} \text{kpc}^2/\text{s}; \quad \delta = 0.85; \quad V_c = 1.35 \times 10^6 \text{cm/s}; \quad L_{max} = 1 \text{kpc}, \quad (50)$$

reduces the antiproton flux by a factor of five. This would make the antiproton bounds comparable to the neutrino ones for $m_\lambda = 5$ TeV, and irrelevant for $m_\lambda = 1$ TeV. (It is of course also possible to choose propagation parameters which magnify the antiproton flux.) Thus, the antiproton bounds should be taken with a grain of salt. In the following, we continue using the more robust Super-Kamiokande constraints as the reference point for estimating the indirect signals of dark matter.

6.3 Other constraints: photons, positrons

Our decaying dark matter particle contributes also to the cosmic flux of positrons and photons. Hard positrons are produced together with W bosons in three-body decays and, to a lesser extent, by subsequent decays of W , Z , and Higgs. Gamma ray photons are produced via decays of W , Z , and Higgs, from final state radiation off charged particles, and through inverse Compton scattering of the hard positrons and electrons on starlight. Below we compute the fluxes of hard positrons and photons from the three-body decay modes and argue that the corresponding bounds are far weaker than those from neutrinos and antiprotons. Therefore, the PAMELA positron measurements and the gamma ray

measurements from FERMI and HESS do not impose new constraints on the lifetime of our dark matter particle.

The positron flux at the Earth due to the positrons from three-body decays is given by [32]

$$\frac{d\Phi_{e^+}}{dE} = \frac{\Gamma_{3b}}{m_\lambda} \frac{1}{2\pi b(E)} \rho_{DM}(r_\odot) \int_E^{m_\lambda/2} dE' \frac{dN_{e^+}}{dE'} I(E; E') \quad (51)$$

Here, the energy loss coefficient $b(E)$ gives the rate of energy loss due to scattering off of cosmic photons and magnetic fields, and is approximately given by $b(E) = \tau_E E^2 / \text{GeV}$ where $\tau_E = 10^{16}$ s. The function $I(E; E')$, sometimes called the halo function, results from semi-analytically solving the diffusion equation for positrons [32]. It is analogous to the function $R(E)$ for antiprotons, and similarly depends on the choice of propagation model. Finally, dN_{e^+}/dE is the positron spectrum from three-body decays, given by

$$\frac{1}{\Gamma_{3b}} \frac{d\Gamma_{3b}}{dE} = \frac{32}{m_\lambda^4} E^2 \left(m_\lambda - \frac{2}{3} E \right). \quad (52)$$

To obtain the positron fraction one has to divide the flux in Eq. (51) by the total flux of electrons and positrons, for which we take

$$\frac{d\Phi_{e^\pm}}{dE} = \frac{0.012}{E^3} \text{ 1}/(\text{cm}^2 \text{ sec GeV}) \quad (53)$$

as measured by FERMI [3]. As an example, in Fig. 6 we plot the contribution to the positron fraction from the three-body decays for $m_\lambda = 2$ TeV, using the MED propagation parameters. We took the decay rate Γ_{3b}/m_λ to be the maximum one allowed by the neutrino bounds from Super-Kamiokande. Recall that for these parameters antiprotons are overproduced by a factor of 2–3. On the other hand, the positron fraction for the same propagation parameters is a factor of 2–4 below that measured by PAMELA. We conclude that positrons do not impose any new constraints on the lifetime of our dark matter particle. At the same time, we cannot explain the anomalous positron fraction via the positrons from three-body decays; another primary source of positrons is needed to explain the PAMELA positron measurement. The new source could be of purely astrophysical origin [33], but it could be glueball (or meson) decays in our model.

Similarly, the contribution to the gamma ray spectrum from the three-body decays is well below the current observational bounds. As an example, we calculate the contribution to the diffuse gamma ray spectrum at intermediate galactic latitudes. Recently, FERMI published the gamma ray spectrum between 0.1 and 10 GeV from between 10 and 20 degrees galactic latitude [34]. The contribution of three-body decays to that spectrum is given by

$$\frac{d\Phi_\gamma}{dE} = 2 \frac{\Gamma_{3b}}{m_\lambda} \frac{dN_\gamma}{dE} I_d(10^\circ, 20^\circ) \quad I_d(\psi_1, \psi_2) = \frac{1}{4\pi} \int_0^{2\pi} d\phi \int_0^\infty dl \int_{\cos \psi_1}^{\cos \psi_2} d \cos \theta \rho_{DM}(r) \quad (54)$$

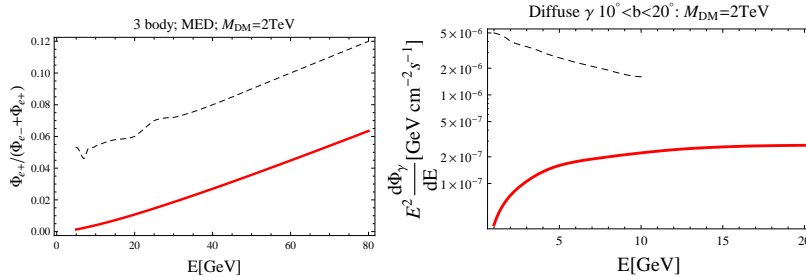


Figure 6: Contributions from three-body decays to positron and gamma ray fluxes for $m_\lambda = 2$ TeV. Left: the positron fraction (solid red) compared to the PAMELA measurement (dashed). Right: the diffuse gamma ray flux $10^\circ < b < 20^\circ$, $0 \leq l \leq 360^\circ$ (solid red) compared to the FERMI measurement (dashed).

where $r = \sqrt{r_\odot^2 + l^2 - 2rl \cos \theta \cos \phi}$. Using Pythia, we determined the photon spectrum dN_γ/dE from W , Z , and Higgs decays, where the parent bosons originate from the three-body decays of dark matter. The results for $m_\lambda = 2$ TeV are plotted in Fig. 6. It is clear that the contribution of the three-body decays is more than an order of magnitude smaller than the flux measured by FERMI. Similarly, the contribution to the gamma ray flux from the galactic center is far below the flux measured by FERMI and HESS [35]. Thus, the strongest constraints on the dark matter lifetime in our model are the galactic center neutrino measurement by Super-Kamiokande and the cosmic antiproton flux measurement by PAMELA.

7 Discovery at Neutrino Telescopes

Our model predicts a monochromatic flux of high-energy ($E_\nu \sim$ TeV) neutrinos and antineutrinos from the galactic center,

$$\frac{d\Phi_\nu}{dE}(\psi) = \frac{d\Phi_{\bar{\nu}}}{dE}(\psi) = \frac{\Gamma_{2b}}{m_\lambda} \delta(E - m_\lambda/2) \frac{r_\odot \rho_\odot}{4\pi} \Delta J_{ls}(\psi), \quad (55)$$

where the line-of-sight integral over the dark matter density profile $\Delta J_{ls}(\psi)$ is given in Eq. (39). The normalization of the flux is set by the dark matter lifetime, Γ_{2b} . The flux is equally populated by all three species of neutrinos; the flux of muon neutrinos to which experiments are most sensitive is one third of Eq. (55). The Super-Kamiokande results place constraints on the dark matter lifetime Γ_{2b}/m_λ , as shown in figure Fig. 4. The dark matter lifetime is also constrained by the antiprotons produced in subdominant three-body decay modes. While the limits on cosmic antiprotons can be comparable to or more stringent than the bounds from Super-Kamiokande, depending on the choice of model for charged

particle propagation in the galaxy, to discuss signals at neutrino telescopes we will continue to use the limits on the dark matter lifetime set by Super-Kamiokande. In this section we discuss the sensitivity of the ANTARES and IceCube neutrino telescopes to the primary neutrino signal. Both experiments have the potential to discover this signal.

7.1 ANTARES

ANTARES is a high-energy neutrino telescope located in the Mediterranean sea. The flux of muon neutrinos from the galactic center produces upward-going muons via charged current interactions in the rock and water below the detector, which ANTARES observes via the Cherenkov light produced in sea water by the muons. The effective detector area $A_{eff}(E)$ for muon neutrinos can be found e.g. in [36] and at 1 TeV is given approximately by 50cm^2 . The energy resolution near 1 TeV is expected to be a factor of 2–3 [37], while the angular resolution is better than a degree and limited mostly by the kinematics of the charged current interactions [36].

The number of signal counts per second from the cone of half-angle ψ around the galactic center is given by

$$\frac{dN_{signal}}{dt} = \frac{2}{3} A_{eff}(m_\lambda/2) \frac{\Gamma_{2b} r_\odot \rho_\odot}{m_\lambda 4\pi} \Delta J_{ls}(\psi), \quad (56)$$

and the neutrino energy is $m_\lambda/2$.

The irreducible background for the dark matter decay signal comes from atmospheric muon neutrinos. The combined flux of atmospheric muon neutrinos and anti-neutrinos at 1 TeV is, averaged over angle [38],

$$\left. \frac{d\Phi_{atm}}{dE d\Omega} \right|_{1\text{TeV}} = 2.7 \times 10^{-11} (\text{GeVcm}^2\text{s sr})^{-1}. \quad (57)$$

The atmospheric neutrino spectrum falls as E^{-3} in the energy range of interest, $100\text{ GeV} < E \lesssim 10\text{ TeV}$. In the energy range $500\text{ GeV} < E \lesssim 5\text{ TeV}$ where we expect hard primary neutrinos from decaying dark matter, neutrino telescopes have poor energy resolution. To differentiate signal from background we therefore rely on first, absolute rate, and second, angular variation in the signal. The neutrinos coming from dark matter decay are concentrated at the galactic center, while the spatial variation of the atmospheric neutrino fluxes is well-known and is at most a factor of 2.5 between zenith and horizon [38]. The number of counts per second from atmospheric neutrinos in a given energy bin E_{min}, E_{max} is given by

$$\frac{dN_{atm}}{dt d\Omega} = \int_{E_{min}}^{E_{max}} dE A_{eff}(E) \frac{d\Phi_{atm}}{dE d\Omega} \quad (58)$$

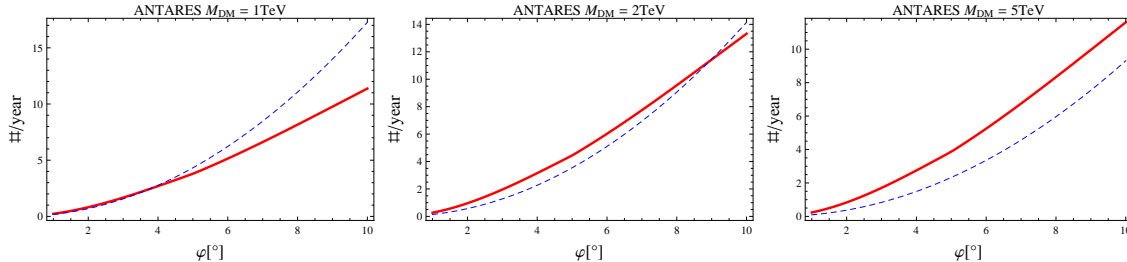


Figure 7: Neutrino counts per year in Antares from the signal (solid red) and the background of atmospheric neutrinos (dashed blue) as a function of the halfangle ψ around the galactic center, for $m_\lambda = 1, 2,$ and 5 TeV. The normalization of the flux corresponds to the maximal flux allowed by Super-Kamiokande for a given dark matter mass.

We approximate the energy resolution of ANTARES by choosing an energy bin $m_\lambda/6 < E < 3m_\lambda/2$, corresponding to a factor of three in energy resolution centered on the energy of the primary neutrino signal. In Fig. 7 we plot the number of signal and background counts per year in this bin for cones around the galactic center as a function of the cone half-angle. We show plots for $m_\lambda = 1, 2,$ and 5 TeV. To generate these plots, we assume that the detector effective area A_{eff} already incorporates factors accounting for detection efficiency and the different cross sections of neutrinos and anti-neutrinos. We use the atmospheric $\nu_\mu + \nu_{\bar{\mu}}$ flux $d\Phi_{atm}/dEd\Omega$ computed in [38] and averaged over the zenith angle. For the signal, we show expected counts for the maximal decay rate allowed by the Super-Kamiokande bounds. For that signal rate, the five-degree cone corresponds to on the order of 5 signal counts and a signal-to-background ratio in the range of 1–3 (for 1–5 TeV dark matter). Thus, in the best case scenario, a clear signal can be detected already in one year of ANTARES data. If no signal is detected, ANTARES can significantly improve the bounds on the dark matter lifetime in our scenario. The theoretical uncertainty in the atmospheric neutrino flux is of order 25 percent at 1 TeV [38]. From that we estimate that one year of ANTARES data can improve the bounds on Γ_{2b} by a factor of 4 to 8, depending on the dark matter mass.

7.2 IceCube

While IceCube, located at the South Pole, has better exposure to the Northern Hemisphere, the extension DeepCore, planned for 2010, will allow IceCube to observe the Southern Hemisphere sky [39]. IceCube’s new sensitivity to the galactic center opens many exciting possibilities for dark matter studies [5]. DeepCore adds additional instrumentation in the clearest and best-shielded portion of the IceCube detector, and enables study of

downward-going neutrinos by using the remainder of the IceCube detector to veto cosmic muons. Cosmic downward-going neutrino signals then consist of neutrino-initiated events with initial interaction vertices located within the fiducial volume of DeepCore.

Muon neutrinos are primarily detected in DeepCore as they are in Super-Kamiokande and ANTARES, as a track from the muon produced in a charged-current interaction of the neutrino with matter. In addition to these *track-like events*, the neutral-current interactions of neutrinos with all flavor, as well as the charged-current interactions of electron and tau neutrinos, deposit energy in a localized region and are reconstructed as *cascade-like events*. Cosmic neutrinos, and in particular neutrinos from dark matter decay, populate all three flavors equally. Usually at neutrino telescopes, the effective volume probed by muon neutrinos is orders of magnitude larger than the effective volume seen by electron and tau neutrinos, due to the large muon penetration depth. However, when using DeepCore to observe downward-going neutrinos, the volume available for muon neutrino events is equal to the volume available for electron and tau neutrino events, putting observable signal events from all three neutrino flavors on an equal footing. While angular resolution for cascade events is less than angular resolution for tracks [39], the high rate of cascade events predicted by our model suggests another potential handle for discovery.

The fiducial volume of DeepCore is estimated to be around 20 megatons [39, 40], that is $V_F \approx 0.02 \text{ km}^3$. Detection efficiencies for neutrino-initiated events are estimated to be 20%–30% [39]. While the angular resolution that can be achieved for DeepCore-initiating events is still to be determined, a reasonable goal is 10 degrees for tracks, possibly improving to 5 degrees, and 40 degrees for cascades [41]. We will estimate the energy resolution to be $r_t = 0.5$ in $\log E$ for tracks and $r_c = 0.3$ in $\log E$ for cascades [41]. The number of neutrino-initiated muons in DeepCore from a given incident neutrino flux is

$$\frac{dN_\mu}{dt d\Omega} = \int dE_\mu \int dE_\nu \alpha_F V_F \sum_N n_N \left(\frac{d\Phi_\nu}{dE_\nu d\Omega} \frac{d\sigma_{\nu N}}{dE_\mu} + \frac{d\Phi_{\bar{\nu}}}{dE_\nu d\Omega} \frac{d\sigma_{\bar{\nu} N}}{dE_\mu} \right). \quad (59)$$

The sum runs over nucleons, $N = n, p$. We take ice to have a density 0.92 g/cm^3 , corresponding to the nucleon number densities $n_n \approx 1.9 \times 10^{-18} \text{ GeV}^3$, $n_p \approx 2.4 \times 10^{-18} \text{ GeV}^3$. We include a factor $\alpha_F = 0.25$ to account for the detection efficiency. The integral over the neutrino energy is trivial for the signal; for the background we set the lower integration limits at $E_\nu = e^{-r_{t,c}} m_\lambda / 2$ for tracks and cascades respectively.

In Fig. 8 we plot the expected number of DeepCore-initiating track-like events originating within a cone of given half-angle around the galactic center. For the maximal signal flux allowed by the Super-Kamiokande constraints, one expects on the order of 25 (5) counts per year inside a cone of half-angle 30° for a dark matter mass of 1 (5) TeV. The dominant background from muon atmospheric neutrinos, also plotted in Fig. 8, gives roughly the

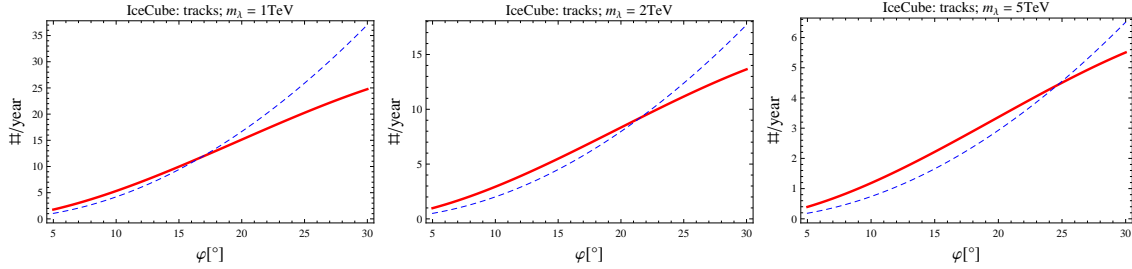


Figure 8: Track-like events per year in DeepCore due to the signal (solid red) and the background of atmospheric muon neutrinos (dashed blue) as a function of the half-angle ψ around the galactic center, for $m_\lambda = 1, 2,$ and 5 TeV. The normalization of the flux corresponds to the maximal flux allowed by Super-Kamiokande for a given dark matter mass.

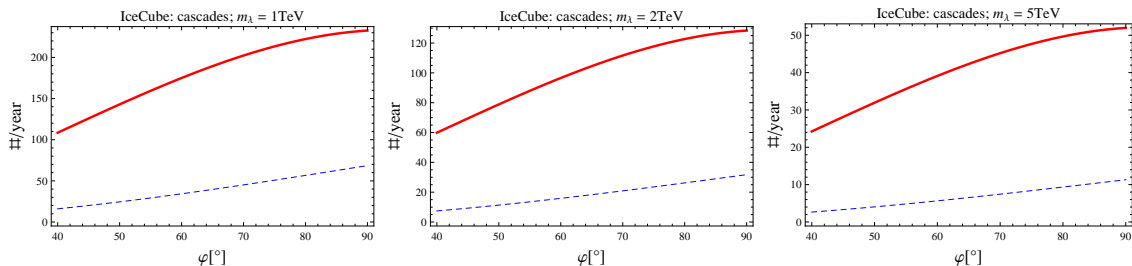


Figure 9: Cascade-like events per year in DeepCore due to the signal (solid red) and the background of atmospheric neutrinos (dashed blue) as a function of the halfangle ψ around the galactic center, for $m_\lambda = 1, 2,$ and 5 TeV. The normalization of the flux corresponds to the maximal flux allowed by Super-Kamiokande for a given dark matter mass.

same number of track-like events as the signal. However, it may be possible to reduce as much as 99 percent of the atmospheric neutrino background by vetoing on the associated collinear muon [42]. If that proves to be the case, the background could be almost completely suppressed and the discovery prospects for the signal are greatly enhanced. The sensitivity of IceCube would only be limited by statistics, and could reach a lifetime of 10^{27} seconds after several years of operation, two orders of magnitude better than the current bounds.

We also compute the number of cascade-like events initiated by the signal and compare to events from the atmospheric neutrino background. As the atmospheric electron neutrino flux is approximately 5 percent of the atmospheric muon neutrino flux in the energy range of interest, the background is dominated by the neutral-current interactions of atmospheric muon neutrinos. Charged-current interactions of atmospheric electron neutrinos contribute

approximately an eighth of the total background event rate. For cascade events, rate alone can serve to distinguish signal from background, as the signal to background ratio can be much larger than one for decay rates near the Super-Kamiokande bounds. In Fig. 9 we plot signal and background rates for cascade events for $m_\lambda = 1, 2,$ and 5 TeV, for the maximal signal flux allowed by the Super-Kamiokande bounds. Again, it may be possible to nearly eliminate the background due to atmospheric muon neutrinos, which would reduce the background by nearly 90 percent. Thus cascade-like events, even more than track-like events, offer powerful handles on neutrino signals of this nature. More importantly, observing an excess of both tracks and cascades would be an important confirmation of the galactic origin of the neutrino flux.

8 Conclusions

We presented a scenario where decay of hidden sector dark matter can give a large flux of neutrinos from the galactic center, dominating over signals in more standard detection channels. Fluxes of the more readily observed e^\pm , antiprotons, and photons are subleading. Observational bounds on the flux of cosmic antiprotons are stringent, and despite the relatively small production rate of antiprotons in this class of model, these observations can become constraining if the lifetime of the dark matter particle is of order 10^{25} seconds. However, the large astrophysical uncertainties in the galactic propagation model for antiprotons make it difficult to draw any robust conclusions from the antiproton spectrum. Moreover, such a dark matter particle naturally interacts very weakly with nucleons, giving null predictions for direct detection experiments. In these circumstances, neutrino telescopes become the most sensitive probe of dark matter.

In the example model we present here, the dark matter candidate is a fermion belonging to a hidden sector which is neutral under all standard model symmetries. Such a particle naturally couples to the standard model via the neutrino portal, which is the lowest-dimensional fermionic gauge singlet operator. The coupling through the neutrino portal enables dark matter to decay to the standard model. The existence of lighter states in the dark sector allows the decay channel with a single standard model neutrino to dominate the final state. This decay mode results in a monoenergetic flux of cosmic neutrinos that can be probed by neutrino telescopes. While we have studied a specific realization of that scenario, where the hidden sector consists of a confining $SU(N)$ gauge group together with a heavy fermion in the adjoint representation, obviously similar phenomenology can be obtained in a wider class of models.

Currently, the coupling via the neutrino portal is most robustly constrained by Super-

Kamiokande, which restricts the dark matter lifetime to be larger than 10^{25} seconds. The PAMELA measurement of the antiproton flux yields roughly comparable constraints due to the antiprotons arising from the subleading dark matter decay channels containing gauge and Higgs bosons. These bounds leave a lot of room for discovery at the current generation of neutrino telescopes. The good angular resolution of both ANTARES and IceCube/DeepCore ensure that the number of signal counts from the direction of the galactic center may be larger than or comparable to the expected background from atmospheric neutrinos. In the case of ANTARES, the sensitivity to the dark matter decay rate exceeds that of Super-Kamiokande by a factor of several. Furthermore, IceCube/DeepCore has the additional prospect of rejecting the vast majority of atmospheric neutrino events by observing the associated muon (which is impossible at ANTARES). This implies increased sensitivity by another order of magnitude with respect to ANTARES.

Our analysis of the sensitivity of ANTARES and IceCube/DeepCore should be considered only as suggestive of the experiments' ultimate capabilities; the operational parameters of these experiments are subject to ongoing research by the collaborations. It is conceivable that designing search algorithms targeted for a monochromatic neutrino signal can further increase the sensitivity to our scenario.

Acknowledgments

We are grateful to Jim Braun and Tyce DeYoung for providing us with many details concerning the IceCube experiment. We would like to thank Peter Graham, Dan Hooper, Patrick Meade, Michele Papucci, Josh Ruderman, Matt Strassler, Scott Thomas, and Tomer Volansky for helpful conversations. This work was supported in part by DOE grant DE-FG02-96ER40959.

References

- [1] O. Adriani *et al.* [PAMELA Collaboration], “An anomalous positron abundance in cosmic rays with energies 1.5-100 GeV,” *Nature* **458**, 607 (2009) [arXiv:0810.4995 [astro-ph]].
- [2] J. Chang *et al.*, “An Excess Of Cosmic Ray Electrons At Energies Of 300-800 GeV,” *Nature* **456**, 362 (2008).
- [3] A. A. Abdo *et al.* [The Fermi LAT Collaboration], “Measurement of the Cosmic Ray e^+ plus e^- spectrum from 20 GeV to 1 TeV with the Fermi Large Area Telescope,” *Phys. Rev. Lett.* **102**, 181101 (2009) [arXiv:0905.0025 [astro-ph.HE]].

- [4] P. Meade, M. Papucci and T. Volansky, “Dark Matter Sees The Light,” arXiv:0901.2925 [hep-ph].
- [5] D. Spolyar, M. Buckley, K. Freese, D. Hooper and H. Murayama, “High Energy Neutrinos As A Test of Leptophilic Dark Matter,” arXiv:0905.4764 [astro-ph.CO]. M. R. Buckley, K. Freese, D. Hooper, D. Spolyar and H. Murayama, “High-Energy Neutrino Signatures of Dark Matter Decaying into Leptons,” arXiv:0907.2385 [astro-ph.HE]. J. T. Ruderman and T. Volansky, “Searching for Smoking Gun Signatures of Decaying Dark Matter,” arXiv:0907.4373 [hep-ph].
- [6] D. E. Kaplan, M. A. Luty and K. M. Zurek, “Asymmetric Dark Matter,” Phys. Rev. D **79**, 115016 (2009) [arXiv:0901.4117 [hep-ph]].
- [7] M. J. Strassler and K. M. Zurek, “Echoes of a hidden valley at hadron colliders,” Phys. Lett. B **651**, 374 (2007) [arXiv:hep-ph/0604261].
- [8] C. J. Morningstar and M. J. Peardon, “The glueball spectrum from an anisotropic lattice study,” Phys. Rev. D **60**, 034509 (1999) [arXiv:hep-lat/9901004].
- [9] M. Gockeler, R. Horsley, A. C. Irving, D. Pleiter, P. E. L. Rakow, G. Schierholz and H. Stuben, “A determination of the Lambda parameter from full lattice QCD,” Phys. Rev. D **73**, 014513 (2006) [arXiv:hep-ph/0502212].
- [10] H. Baer, K. m. Cheung and J. F. Gunion, “A Heavy gluino as the lightest supersymmetric particle,” Phys. Rev. D **59**, 075002 (1999) [arXiv:hep-ph/9806361].
- [11] A. Arvanitaki, C. Davis, P. W. Graham, A. Pierce and J. G. Wacker, “Limits on split supersymmetry from gluino cosmology,” Phys. Rev. D **72**, 075011 (2005) [arXiv:hep-ph/0504210].
- [12] H. K. Dreiner, H. E. Haber and S. P. Martin, “Two-component spinor techniques and Feynman rules for quantum field theory and supersymmetry,” arXiv:0812.1594 [hep-ph].
- [13] E. Komatsu *et al.* [WMAP Collaboration], “Five-Year Wilkinson Microwave Anisotropy Probe (WMAP) Observations:Cosmological Interpretation,” Astrophys. J. Suppl. **180**, 330 (2009) [arXiv:0803.0547 [astro-ph]].
- [14] J. Kang, M. A. Luty and S. Nasri, “The Relic Abundance of Long-lived Heavy Colored Particles,” JHEP **0809**, 086 (2008) [arXiv:hep-ph/0611322].

- [15] J. Hisano, S. Matsumoto and M. M. Nojiri, “Explosive dark matter annihilation,” *Phys. Rev. Lett.* **92**, 031303 (2004) [arXiv:hep-ph/0307216]. J. Hisano, S. Matsumoto, M. Nagai, O. Saito and M. Senami, “Non-perturbative Effect on Thermal Relic Abundance of Dark Matter,” *Phys. Lett. B* **646**, 34 (2007) [arXiv:hep-ph/0610249]. A. Strumia, “Sommerfeld corrections to type-II and III leptogenesis,” *Nucl. Phys. B* **809**, 308 (2009) [arXiv:0806.1630 [hep-ph]].
- [16] R. Dave, D. N. Spergel, P. J. Steinhardt and B. D. Wandelt, “Halo Properties in Cosmological Simulations of Self-Interacting Cold Dark Matter,” *Astrophys. J.* **547**, 574 (2001) [arXiv:astro-ph/0006218].
- [17] O. Y. Gnedin and J. P. Ostriker, “Limits on Collisional Dark Matter from Elliptical Galaxies in Clusters,” *Astrophys. J.* **561**, 61 (2001) [arXiv:astro-ph/0010436].
- [18] M. Markevitch *et al.*, “A Textbook Example of a Bow Shock in the Merging Galaxy Cluster 1E0657-56,” *Astrophys. J.* **567**, L27 (2002) [arXiv:astro-ph/0110468].
- [19] S. W. Randall, M. Markevitch, D. Clowe, A. H. Gonzalez and M. Bradac, “Constraints on the Self-Interaction Cross-Section of Dark Matter from Numerical Simulations of the Merging Galaxy Cluster 1E 0657-5,” arXiv:0704.0261 [astro-ph].
- [20] Y. Chen *et al.*, “Glueball spectrum and matrix elements on anisotropic lattices,” *Phys. Rev. D* **73**, 014516 (2006) [arXiv:hep-lat/0510074].
- [21] J. E. Juknevich, D. Melnikov and M. J. Strassler, “A Pure-Glue Hidden Valley I. States and Decays,” arXiv:0903.0883 [hep-ph].
- [22] J. F. Navarro *et al.*, “The Inner Structure of LambdaCDM Halos III: Universality and Asymptotic Slopes,” *Mon. Not. Roy. Astron. Soc.* **349**, 1039 (2004) [arXiv:astro-ph/0311231].
- [23] J. F. Navarro, C. S. Frenk and S. D. M. White, “A Universal Density Profile from Hierarchical Clustering,” *Astrophys. J.* **490**, 493 (1997) [arXiv:astro-ph/9611107].
- [24] S. Desai *et al.* [Super-Kamiokande Collaboration], “Search for dark matter WIMPs using upward through-going muons in Super-Kamiokande,” *Phys. Rev. D* **70**, 083523 (2004) [Erratum-ibid. D **70**, 109901 (2004)] [arXiv:hep-ex/0404025].
- [25] S. Desai *et al.* [Super-Kamiokande Collaboration], “Study of TeV Neutrinos with Upward Showering Muons in Super-Kamiokande,” *Astropart. Phys.* **29**, 42 (2008) [arXiv:0711.0053 [hep-ex]].

- [26] D. E. Groom, N. V. Mokhov and S. I. Striganov, “Muon stopping power and range tables 10-MeV to 100-TeV,” *Atom. Data Nucl. Data Tabl.* **78**, 183 (2001).
- [27] P. Lipari and T. Stanev, “Propagation Of Multi - Tev Muons,” *Phys. Rev. D* **44**, 3543 (1991).
- [28] F. Donato, D. Maurin, P. Salati, A. Barrau, G. Boudoul and R. Taillet, “Antiprotons from spallation of cosmic rays on interstellar matter,” *Astrophys. J.* **563**, 172 (2001) [arXiv:astro-ph/0103150].
- [29] J. Hisano, S. Matsumoto, O. Saito and M. Senami, “Heavy Wino-like neutralino dark matter annihilation into antiparticles,” *Phys. Rev. D* **73**, 055004 (2006) [arXiv:hep-ph/0511118].
- [30] F. Donato, N. Fornengo, D. Maurin and P. Salati, “Antiprotons in cosmic rays from neutralino annihilation,” *Phys. Rev. D* **69**, 063501 (2004) [arXiv:astro-ph/0306207].
- [31] A. Barrau, G. Boudoul, F. Donato, D. Maurin, P. Salati and R. Taillet, “Antiprotons from primordial black holes,” *Astron. Astrophys.* **388**, 676 (2002) [arXiv:astro-ph/0112486].
- [32] T. Delahaye, R. Lineros, F. Donato, N. Fornengo and P. Salati, “Positrons from dark matter annihilation in the galactic halo: theoretical uncertainties,” *Phys. Rev. D* **77**, 063527 (2008) [arXiv:0712.2312 [astro-ph]].
- [33] D. Grasso *et al.* [FERMI-LAT Collaboration], “On possible interpretations of the high energy electron-positron spectrum measured by the Fermi Large Area Telescope,” arXiv:0905.0636 [astro-ph.HE].
- [34] T. A. Porter and f. t. F. Collaboration, “Fermi LAT Measurements of the Diffuse Gamma-Ray Emission at Intermediate Galactic Latitudes,” arXiv:0907.0294 [astro-ph.HE].
- [35] F. Aharonian *et al.* [H.E.S.S. Collaboration], “Discovery of Very-High-Energy Gamma-Rays from the Galactic Centre Ridge,” *Nature* **439**, 695 (2006) [arXiv:astro-ph/0603021]. F. Aharonian *et al.* [H.E.S.S. Collaboration], “HESS observations of the galactic center region and their possible dark matter interpretation,” *Phys. Rev. Lett.* **97**, 221102 (2006) [Erratum-ibid. **97**, 249901 (2006)] [arXiv:astro-ph/0610509].

- [36] A. M. Brown and f. t. A. Collaboration, “The ANTARES Neutrino Telescope: status and first results,” arXiv:0908.1035 [astro-ph.HE].
- [37] J. P. Ernenwein, “The ANTARES neutrino telescope,” *To appear in the proceedings of 40th Rencontres de Moriond on Electroweak Interactions and Unified Theories, La Thuile, Aosta Valley Italy, 5-12 Mar 2005.*
- [38] M. Honda, T. Kajita, K. Kasahara, S. Midorikawa and T. Sanuki, “Calculation of atmospheric neutrino flux using the interaction model calibrated with atmospheric muon data,” Phys. Rev. D **75**, 043006 (2007) [arXiv:astro-ph/0611418].
- [39] E. Resconi and f. t. I. Collaboration, “Status and prospects of the IceCube neutrino telescope,” Nucl. Instrum. Meth. A **602**, 7 (2009) [arXiv:0807.3891 [astro-ph]].
- [40] C. Wiebusch and f. t. I. Collaboration, “Physics Capabilities of the IceCube DeepCore Detector,” arXiv:0907.2263 [astro-ph.IM].
- [41] T. DeYoung, private communication.
- [42] S. Schonert, T. K. Gaisser, E. Resconi and O. Schulz, “Vetoing atmospheric neutrinos in a high energy neutrino telescope,” arXiv:0812.4308 [astro-ph].